Dyrk1A haploinsufficiency affects viability and causes developmental delay and abnormal brain morphology in mice

MOLECULAR AND CELLULAR BIOLOGY, Sept. 2002, p. 6636–6647 Vol. 22, No. 18
0270-7306/02/$04.00+0 DOI: 10.1128/MCB.22.18.6636–6647.2002

Dyrk1A Haploinsufficiency Affects Viability and Causes Developmental Delay and Abnormal Brain Morphology in Mice

Vassiliki Fotaki,[1,2] Mara Dierssen,[1,2] Soledad Alcántara,[3] Salvador Martínez,[4] Eulàlia Martí,[1,2] Caty Casas,[1]† Joana Visa,[1]‡ Eduardo Soriano,[3] Xavier Estivill,[1,2] and Maria L. Arbonés[1,2]*

Medical and Molecular Genetics Center, Institut de Recerca Oncològica, 08907-L'Hospitalet de Llobregat, Barcelona[1], Genes and Disease Program, Centre de Regulació Genòmica, 08003-Barcelona[2], Department of Cell Biology and Neuroscience Research Center (CERN), University of Barcelona, 08028-Barcelona,[3] and Instituto de Neurociencias de Alicante, Universidad Miguel Hernández-CSIC, 03550-Alicante,[4] Spain

Received 18 April 2002/Returned for modification 3 June 2002/Accepted 13 June 2002

***DYRK1A* is the human orthologue of the *Drosophila minibrain* (*mnb*) gene, which is involved in postembryonic neurogenesis in flies. Because of its mapping position on chromosome 21 and the neurobehavioral alterations shown by mice overexpressing this gene, involvement of DYRK1A in some of the neurological defects of Down syndrome patients has been suggested. To gain insight into its physiological role, we have generated mice deficient in Dyrk1A function by gene targeting. Dyrk1A$^{-/-}$ null mutants presented a general growth delay and died during midgestation. Mice heterozygous for the mutation (Dyrk1A$^{+/-}$) showed decreased neonatal viability and a significant body size reduction from birth to adulthood. General neurobehavioral analysis revealed preweaning developmental delay of Dyrk1A$^{+/-}$ mice and specific alterations in adults. Brains of Dyrk1A$^{+/-}$ mice were decreased in size in a region-specific manner, although the cytoarchitecture and neuronal components in most areas were not altered. Cell counts showed increased neuronal densities in some brain regions and a specific decrease in the number of neurons in the superior colliculus, which exhibited a significant size reduction. These data provide evidence about the nonredundant, vital role of *Dyrk1A* and suggest a conserved mode of action that determines normal growth and brain size in both mice and flies.**

Dual-specificity tyrosine-regulated kinases (DYRKs) are a novel subfamily of protein kinases that catalyze their autophosphorylation on tyrosine residues and the phosphorylation of serine/threonine residues on exogenous substrates (5, 7, 19). Their kinase activity depends on the presence of a YXY motif in the activation loop of the catalytic domain (20), which is located at the same position as the characteristic TXY motif of the mitogen-activated protein kinases (MAPKs), indicating a possible involvement of these proteins in signal transduction pathways similar to those of the MAPKs (26).

Lower eukaryotic members of this family are the kinases Yak1p in *Saccharomyces cerevisiae* (13), Pom1p in *Schizosaccharomyces pombe* (4), and YakA in *Dictyostelium discoideum* (33). Although strains with mutations in these proteins present different phenotypic abnormalities, they all seem to be involved in cell cycle regulation and the control of the cell transition from growth to differentiation. The DYRK protein of *Drosophila melanogaster*, called minibrain (mnb), is implicated in postembryonic neurogenesis. Mutant flies with reduced mnb expression present reductions in the volumes of the adult optic lobes and central brain hemispheres, due to abnormal spacing of neuroblasts in the outer proliferation center of the larval brain (34). Mammalian DYRKs include DYRK1A, DYRK1B (or MIRK), DYRK2, DYRK3, and DYRK4 (6). DYRK1A is the most extensively characterized member of this family, and it shares all the characteristic motifs of the catalytic domain with the other family members. Outside the catalytic domain it presents some special features, such as a bipartite nuclear localization signal, a PEST sequence, a histidine repeat, and a region rich in serine-threonine residues (20).

The human *DYRK1A* gene maps to chromosome 21 (HSA21) in the Down syndrome (DS) critical region 21q22.2 (16, 29, 32). Part of this region includes the chromosomal segment deleted in HSA21-linked microcephaly (24). The mouse *Dyrk1A* gene maps to chromosome 16, in the region of synteny with HSA21 (31). The human *DYRK1A* and rodent *Dyrk1A* genes are ubiquitously expressed in tissues of adult and fetal origin (16, 32), with high expression levels in the brain and heart during development (27). In addition, *DYRK1A* is overexpressed in DS fetal brains, while its mouse orthologue is overexpressed in the brains of adult Ts65Dn mice (15), a partial trisomy 16 mouse model, widely used as a model for DS (11). All these data suggest that *DYRK1A* might be one of the genes involved in some of the neurological abnormalities observed in DS patients. In agreement with this is the fact that transgenic mouse models overexpressing the *Dyrk1A* gene present a deficit in visuospatial learning and memory (3, 30).

DYRK1A phosphorylates a variety of substrates in vitro, such as the signal transducer and activator of transcription 3 (STAT3) (25), the ε subunit of eukaryotic initiation factor 2B (eIF2Bε), the microtubule-associated protein tau (35), and the transcription factor of the forkhead family FKHR (36), indicating its possible involvement in more than one biochemical pathway in vivo. The only available data about its in vivo role show that DYRK1A, when activated by the basic fibroblast

* Corresponding author. Mailing address: Centre de Regulació Genòmica, Passeig Marítim 37–49, la planta, 08003-Barcelona, Spain. Phone: (34) 932240900. Fax: (34) 932240899. E-mail: mariona.arbones@crg.es.

† Present address: Aventis-Pharma, 94400-Vitry, France.

‡ Present address: Research Animal Facility, Barcelona Science Park, 08028-Barcelona, Spain.

growth factor (bFGF) in immortalized hippocampal progenitor cells, stimulates the phosphorylation of the cyclic AMP response element binding protein (CREB) and induces subsequent CRE-mediated gene transcription. In addition, overexpression of a kinase-deficient DYRK1A remarkably attenuates the differentiation of hippocampal cells (37). Although the exact role of DYRK1A in central nervous system (CNS) function has not been determined, this recent finding provides the first evidence about the involvement of DYRK1A in neuronal differentiation.

To contribute to the elucidation of the physiological function of DYRK1A, we have performed targeted disruption of the *Dyrk1A* gene in mice. The phenotypic effects of the loss of one and two copies of *Dyrk1A* are presented, providing evidence about the role of DYRK1A in normal growth, development, and CNS function.

MATERIALS AND METHODS

Targeted disruption of *Dyrk1A*. A 15.5-kb clone was isolated from a lambda FIXII genomic library (129 SVJ; Stratagene) by using as a probe a PCR fragment that expands 979 nucleotides (nucleotides 786 to 1768; accession number AF108830) of the human *DYRK1A* cDNA. The insert was mapped and partially sequenced to determine the intron-exon boundaries. The exons contained in the phage clone correspond to exons 5 to 8 of the human gene (15). To construct the targeting vector, a 5′-homology arm of 3.6 kb containing exon 6, a 3′-homology arm of 2.1 kb containing the 3′ end of exon 8, the *PGKneobpA* cassette, and the *PGKtk* cassette were subcloned in several steps into the pSP72 plasmid (Promega). The resulting construct was linearized at the unique *Pvu*I site and electroporated into E14-1 cells as previously described (21). Clones resistant to G418 and ganciclovir were analyzed by Southern blotting using *Eco*RI-digested DNA and a 5′-flanking probe (see Fig. 1). Two correctly recombinant clones (clones 13 and 40) were microinjected into C57BL/6 blastocysts, resulting in male chimeras that were subsequently bred with C57BL/6 females to generate heterozygous offspring. Although the two lines showed identical phenotypes, the data presented were obtained from mice derived from embryonic stem (ES) cell clone 13 on a mixed C57BL/6–129Ola genetic background.

Genotyping mice and embryos. Mice and embryos were genotyped by Southern blotting as shown in Fig. 1C or by PCR analysis by using tail or yolk sac genomic DNA. A combination of the *neo* primer P1 (5′-ATTCGCAGCGCAT CGCCTTCTATCGCC-3′) and the *Dyrk1A* primers P2 (5′CTTATGACAGAG TGGAGCAA-3′) and P3 (5′-CGTGATGAGCCCTTACCTATG-3′) (see Fig. 1B) was used to amplify the wild-type and mutant alleles. PCR comprised denaturation at 96°C for 3 min, followed by 35 cycles of 30 s at 94°C, 35 s at 60°C, and 40 s at 72°C, and a final extension step at 74°C for 10 min.

Reverse transcription-PCR (RT-PCR). Total RNA was isolated from wild-type and Dyrk1A$^{+/-}$ brains by using the Tripure RNA extraction reagent (Roche). Samples (1 μg) were reverse transcribed with a random hexamer primer (Pharmacia) and SuperScript II (Invitrogen) by following the manufacturer's conditions. *Dyrk1A* primers P4 (5′-GAGAGACTTCAGCATGCA-3′) and P5 (5′-CCAACTGACAAGAGCTGCCA-3′) were used for PCR amplification.

Western blot analysis. Proteins were extracted by homogenizing mouse embryos at day 10.5 of gestation (E10.5) in boiling 2× sodium dodecyl sulfate (SDS) sample buffer (22) and separated in an SDS–7.5% PAGE gel. The amount of protein loaded in the gel was standardized by Coomassie brilliant blue staining by using proteins of known concentrations as controls. Proteins were transferred to nitrocellulose membranes (Amersham), and successful transfer was controlled by Ponceau S staining. Membranes were blocked with 5% low-fat milk in phosphate-buffered saline (PBS). Incubations with primary antibodies were carried out in PBS with 3% low-fat milk. Primary antibodies were detected with horseradish peroxidase-conjugated antibodies, and positive signals were visualized with the ECL system (Pierce). As primary antibodies we used a mouse polyclonal antibody raised in our laboratory against the last 144 amino acids of rat Dyrk1A (dilution, 1:250) and a goat polyclonal antibody against the amino terminus of Dyrk1A (G-19; sc-12568; dilution, 1:100; Santa Cruz Biotechnology).

Embryo histology, immunohistochemistry, and in situ hybridization. Dyrk1A$^{+/-}$ mice were mated, and the morning of the vaginal plug was defined as embryonic day 0.5 (E0.5). A minimum of two embryos of each genotype (Dyrk1A$^{+/+}$, Dyrk1A$^{+/-}$, and Dyrk1A$^{-/-}$) from at least two litters were collected at E9.5, E10.5, and E11.5 and fixed in 4% paraformaldehyde in PBS for 24 h at 4°C. Embryos were dehydrated in an ethanol series, cleared in xylene, and embedded in paraffin. Paraffin blocks were serially sectioned (thickness, 10 μm) and stained with cresyl violet. Sections were carefully examined to detect histological differences between wild-type, Dyrk1A$^{+/-}$, and Dyrk1A$^{-/-}$ embryos. Immunohistochemistry was performed after blocking of endogenous peroxidase with 0.03% H_2O_2 solution in PBS for 20 min at 4°C. After three rinses with PBS, sections were washed with four consecutive changes of a solution of 0.1% Triton X-100 in PBS for 10 min each time. Sections were blocked for an hour in blocking solution (0.2% gelatin, 10% normal goat serum, and 0.1% Triton X-100 in PBS) and incubated overnight at 4°C with a monoclonal antibody against β-tubulin (Tuj-1) (Roche) diluted (1:500) in the blocking solution with 5% normal goat serum. Sections were incubated with a biotinylated secondary antibody (dilution, 1:200; Vector Labs) for an hour, and positive signals were developed with a diaminobenzidine substrate by using the avidin-biotin-peroxidase system according to the manufacturer's instructions (Vector Labs).

Whole-mount in situ hybridization was performed essentially as previously described (18). A partial *Dyrk1A* cDNA clone (nucleotides 241 to 590; accession number U58497) was used as a template to generate sense and antisense riboprobes by in vitro transcription with the dioxigenin RNA labeling kit (Roche) by using either T3 or T7 RNA polymerase.

Histology and immunohistochemistry of the nervous system. Adult and PD14 (postnatal day 14) mice were anesthetized and transcardially perfused with 4% paraformaldehyde in 0.1 M phosphate buffer, pH 7.4. Brains were removed and postfixed in the same buffer for 24 h at 4°C. Thereafter, they were cryoprotected in 30% sucrose, frozen on dry ice, and sectioned on a cryostat. Serial coronal or sagittal (30- or 50-μm-thick) sections were collected in a cryoprotectant solution (30% glycerol, 30% ethylene glycol, 40% 0.1 M phosphate buffer [pH 7.4]), and every sixth section was stained with Nissl. Immunohistochemistry was performed for two to five adult or PD14 male mice per genotype as described above (embryo histology). Primary polyclonal antibodies from rabbits were against calbindin (1:10,000), calretinin (1:3,000), parvalbumin (1:5,000) (all from Swant Antibodies), and the glial fibrillary acidic protein (GFAP) (1:2,000) (Dako). Primary monoclonal antibodies from mice were against syntaxin 1 (1:100,000) (HPC.1; Sigma), SNAP 25 (1:2,000) (SMI-81; Stenberger Antibodies), and synaptobrevin (VAM-2) (1:100,000) (Cl.69.1; Synaptic Systems). The rat monoclonal antibody against the myelin proteolipid protein (PLP) was kindly provided by Boris Zalc (INSERM, Paris, France).

Morphometric analysis. Morphometric analysis was performed on three adult male mice per group. After cryoprotection, brains were coronally sectioned (thickness, 50 μm) in a cryostat. For determination of the area of the neuronal soma, profiles of Nissl-stained neurons in layer V of the somatosensory barrel cortex (40× objective) and the stratum griseum superficiale (SGS) of the superior colliculus (SC) (60× objective) (100 to 120 neurons per animal for each region) were traced with the aid of a camera lucida and the areas were calculated by using the IMAT image analysis program (Scientific-Technical Services, University of Barcelona). For quantitative analysis, Nissl-stained sections were analyzed by using a 60× objective and a millimetric eyepiece. Numbers of nuclei in the somatosensory barrel cortex (layers II-III, IV, and V), the thalamus (ventral posteroromedial [VPM]), and the SC (SGS and stratum opticum [SO]) were counted. Counts were carried out in four to eight different visual fields (1 mm^2) in parallel sections for each animal group. All data were statistically analyzed by using the Student *t* test.

Somatometric and neurobehavioral analysis. Mice used for behavioral analysis were derived from crosses between wild-type F_1 females and Dyrk1A$^{+/-}$ F_1 males. Mice were reared under standard conditions on a 12-h light-dark cycle (lights on at 0800 am), at 20 to 22°C and a relative humidity of 50 to 70%, with food and water available ad libitum. The day of birth was considered PD1. After the weaning period, at the age of 3 to 4 weeks, animals were housed as siblings, separated according to sex.

A cohort of 11 Dyrk1A$^{+/+}$ and 7 Dyrk1A$^{+/-}$ mice were examined during the preweaning period. Somatometry was performed daily (PD1 to PD20) by weighing the pups and measuring the body length, from the tip of the nose to the base of the tail, and the length of the tail. The day of appearance of developmental landmarks was recorded and used as the unit of analysis. Neurobehavioral analysis included a battery of tests evaluating preweaning sensorial and motor responses (12) that reflect the maturation of the CNS.

Adult mice (5 to 10 male and female mice per genotype) were weighed weekly from the 4th to the 12th week of age. Postweaning neurobehavioral analysis was performed with a cohort of 23 Dyrk1A$^{+/+}$ and 15 Dyrk1A$^{+/-}$ mice at the age of 3 months. The effect of genotype was evaluated on 35 separate behavioral measurements recorded as part of the SHIRPA primary screen protocol (28),

which provides a comprehensive behavioral profile for each animal. This protocol has been used for high-throughput analysis in a large-scale mouse mutagenesis project and assesses as many as 40 separate measurements for each animal. Full details of the experimental procedures can be found on the website for the Mouse Mutagenesis consortium partners (http://www.mgu.har.mrc.ac.uk/mutabase/shirpa_1.html). Assessment of each animal began with observation of undisturbed behavior in a cylindrical clear Perspex viewing jar (height, 15 cm; diameter, 11 cm). Mice were then transferred to an arena (55 by 33 cm) for observation of motor behavior. This was followed by a sequence of manipulations using tail suspension where measurements of visual acuity, grip strength, body tone, and reflexes were recorded.

Data analysis. When no significant differences were detected between male and female mice of each genotype, results were combined. Unless stated otherwise, the significance of the effects was assessed by a one-way or multivariate analysis of variance (ANOVA) with Bonferroni's post hoc analysis test. Student's *t* test was used for comparisons between two groups. All analyses were performed by using the statistical package SPSS for Windows, version 8.0.

RESULTS

Targeted disruption of the *Dyrk1A* gene in ES cells. We used standard gene-targeting techniques to generate *Dyrk1A*-deficient mice. A 3.2-kb genomic fragment containing exon 7 and most of exon 8 of the mouse *Dyrk1A* gene was replaced with a neomycin resistance (*neo*) gene by homologous recombination. The sequence removed encodes 112 amino acids of Dyrk1A and includes the bipartite nuclear localization signal, a short consensus sequence rich in aspartate residues that is speculated to regulate the kinase activity (5), and the first three subdomains (I to III) of the catalytic domain, which are necessary for ATP binding activity (17) (Fig. 1A and B). Three correctly targeted Dyrk1A$^{+/-}$ ES cell clones were detected by Southern blot analysis using a *Dyrk1A* external probe and were confirmed by using a *neo* probe (Fig. 1C). Two of these clones gave rise to germ line transmission chimeras that were bred to establish the F_1 generation.

To evaluate whether the targeted mutation could result in a new allele, cDNAs obtained from brain RNA of control and Dyrk1A$^{+/-}$ mice were PCR amplified with primers external to the homology arms. Sequencing of the products obtained revealed that the mutant allele generated a new *Dyrk1A* transcript (Fig. 1D). This transcript was the outcome of an aberrant splicing event involving exons 6 and 9, leading to deletion of the *neo* cassette and exon 8. Although a truncated protein of 111 amino acid residues could result from this transcript, no such product was detected by Western blotting using an antibody against the amino terminus of Dyrk1A (data not shown). This protein could be made at undetectable levels, but it would be inactive.

Embryonic mortality of homozygous Dyrk1A$^{-/-}$ mice. Heterozygous Dyrk1A$^{+/-}$ mice of the F_1 generation were underrepresented among weaned pups and were phenotypically distinguishable due to their small body size (discussed in detail below). In spite of these differences, adult heterozygotes appeared healthy and were intercrossed to produce homozygous mice. Genotyping of 51 offspring of such crosses revealed no live homozygous Dyrk1A$^{-/-}$ pups, indicating the lethality of the mutation in embryos.

Previous data had shown the expression pattern of *Dyrk1A* from E13 onward by in situ hybridization, while the expression of the gene had been revealed at E11.5 by Northern blotting (32). To determine at which embryonic stage the homozygous mutants die, we collected embryos from timed pregnant mothers, starting at E9.5. The amniotic sac of each embryo was genotyped by Southern blotting or PCR (Fig. 2A). The results of this analysis revealed that Dyrk1A$^{-/-}$ embryos died between E10.5 and E13.5, with only 20% surviving at E13.5 (Table 1).

Whole-mount in situ hybridization revealed the presence of the *Dyrk1A* transcript in the neural tubes of wild-type E9.5 embryos (Fig. 2B). High expression was observed in the optic vesicle and the ventral neural tube, particularly along the rhombencephalon and spinal cord, while moderate expression was detected in the telencephalic, diencephalic, and mesencephalic vesicles. Strong expression was also observed in the otic vesicle and the branchial arches. No expression was observed in the truncus arteriosus or the bulbus cordis of the developing heart, although the transcript was detected in the wall of the common atrial chamber. No signal was detected in homozygous Dyrk1A$^{-/-}$ embryos when the same antisense probe was used. Western blot analysis of proteins derived from E10.5 embryonic tissues confirmed the absence of the Dyrk1A protein in null embryos and showed a reduction of protein levels in heterozygotes (Fig. 2C).

To study the morphology of the nullizygous embryos, E9.5, E10.5, and E11.5 litters were analyzed by cresyl violet staining of sagittal sections. Dyrk1A$^{-/-}$ embryos presented a significant growth delay, with 1/3 to 1/2 size reduction compared to wild-type littermates. The morphology of the heart, liver primordium, branchial arches, and brain vesicles showed a developmental structural delay (Fig. 2D). In contrast, heterozygous embryos of the same litters presented no significant size reduction or other morphological alteration relative to controls (data not shown). We next performed immunohistochemistry using the anti-β-tubulin antibody, which specifically stains differentiating neuronal cells. Immunostained cells were detected in the neural tubes of E9.5 Dyrk1A$^{+/+}$ embryos, and their number and distribution increased at E10.5 and E11.5. A similar spatiotemporal pattern was observed in Dyrk1A$^{-/-}$ embryos, although the immunostaining was significantly reduced from that for controls. In fact, there was a reduction in the number of immunoreactive postmitotic neurons (Fig. 2E), indicating either a defect in neuroblast proliferation or a delay in the maturation of the nervous systems of Dyrk1A$^{-/-}$ embryos.

Reduced postnatal viability and smaller body size of Dyrk1A$^{+/-}$ mice. To evaluate the effect of Dyrk1A protein reduction on heterozygous mice, we studied the progeny resulting from female Dyrk1A$^{+/+}$ and male Dyrk1A$^{+/-}$ matings. Of 638 pups recorded at the time of birth, only 451 (70%) survived by the end of the preweaning period. The remaining 187 pups (29% of the live-born pups) died during the first 3 days of life. Genotype analysis of the surviving pups showed a 30% reduction in the number of Dyrk1A$^{+/-}$ mice compared to the expected Mendelian ratio. Therefore, we attribute the reduction of the expected number of Dyrk1A$^{+/-}$ mice to neonatal lethality.

Dyrk1A$^{+/-}$ mice that survived to adulthood appeared distinctly smaller than their wild-type littermates (Fig. 3A). They presented a significant reduction in body weight ($F = 285.7$, $df = 25$, and $P < 0.0001$ by ANOVA) and length ($F = 133.4$, $df = 25$, $P < 0.0001$) during the entire preweaning period (Fig. 3B). The body weight curve was shifted to the right in a nonparallel fashion, indicating a progressive increase in the weight

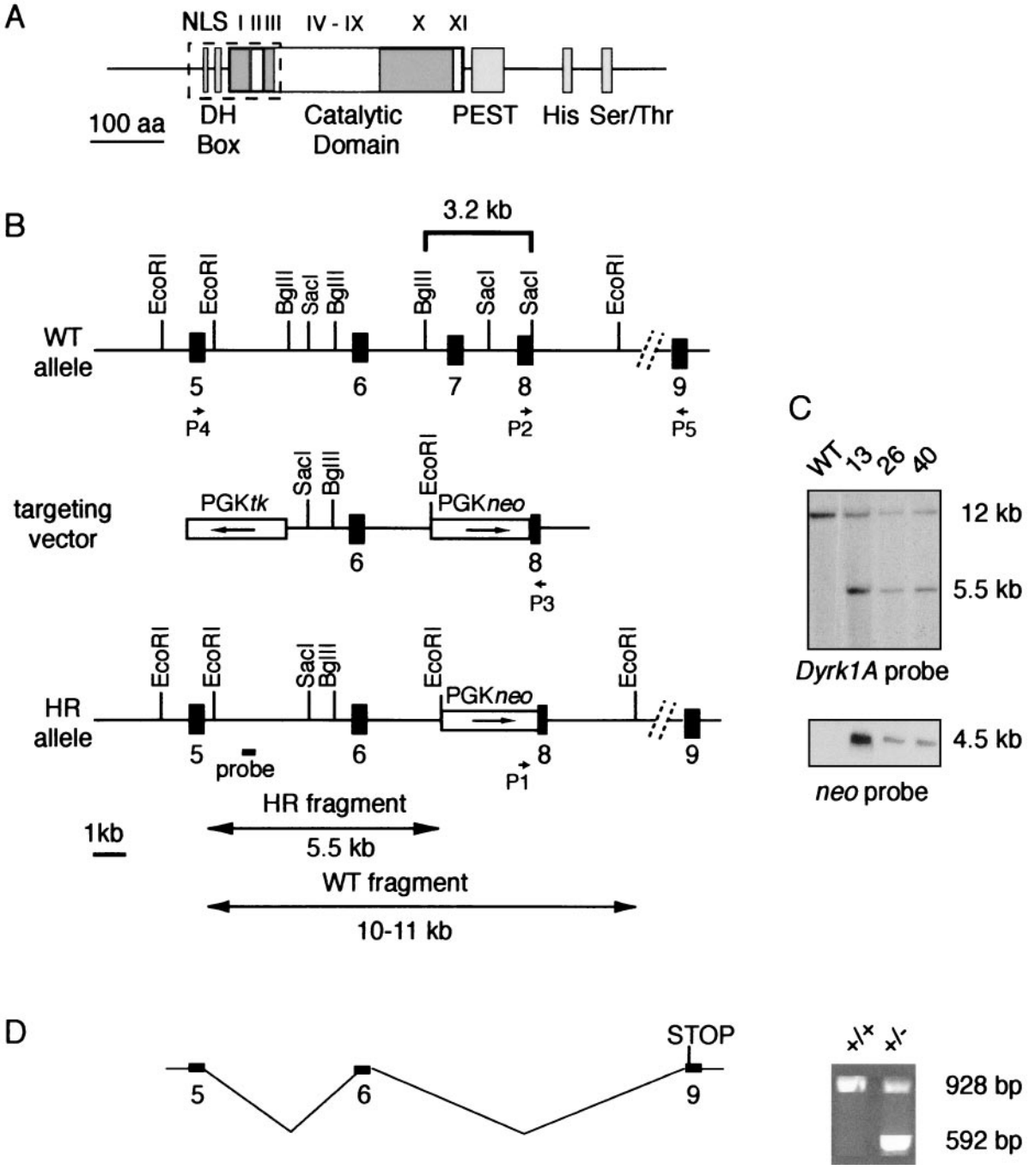

FIG. 1. Targeted disruption of mouse *Dyrk1A* by homologous recombination. (A) Schematic diagram of the Dyrk1A protein. Positions of the catalytic domain and other structural motifs are indicated (NLS, bipartite nuclear localization signal; DH box, consensus sequence rich in aspartate residues; PEST, proline, glutamate, serine, and threonine region; His, histidine repeat; Ser/Thr, serine/threonine repeat; I to XI, subdomains of the catalytic domain). Dashed rectangle indicates the amino acid sequence deleted by gene targeting. (B) Diagram showing the genomic structure of the endogenous wild-type (WT) allele, the targeting vector, and the homologous recombinant (HR) allele. Arrows indicate the transcriptional orientations of the *neo* gene and the *thymidine kinase* (*tk*) gene in the targeting vector. The 5′ flanking probe used for Southern blotting and the expected sizes of the restriction fragments after *Eco*RI digestion of genomic DNA are shown. P1, P2, and P3 indicate the locations of the primers used for PCR analysis (Fig. 2A); P4 and P5 indicate the locations of the primers used for RT-PCR (panel D). (C) Southern blots of *Eco*RI-digested DNA from the wild-type parental ES cell line and three recombinant clones (clones 13, 26, and 40) hybridized with the *Dyrk1A* probe and a *neo* probe. (D) (Right) RT-PCR analysis of adult brain tissue with primers external to the targeting event (exons 5 and 9 in panel B) gave rise to a unique product in wild type (+/+) tissue, whereas an additional, shorter product was generated in Dyrk1A heterozygous (+/−) tissue. The same aberrant transcript was also observed in brain and embryonic tissues of all Dyrk1A$^{+/-}$ mice examined. This resulted from aberrant splicing, which led to the deletion of the *neo* cassette and exon 8 and the introduction of a new stop codon immediately downstream of the targeting event. (Left) Diagram of this alternative transcript.

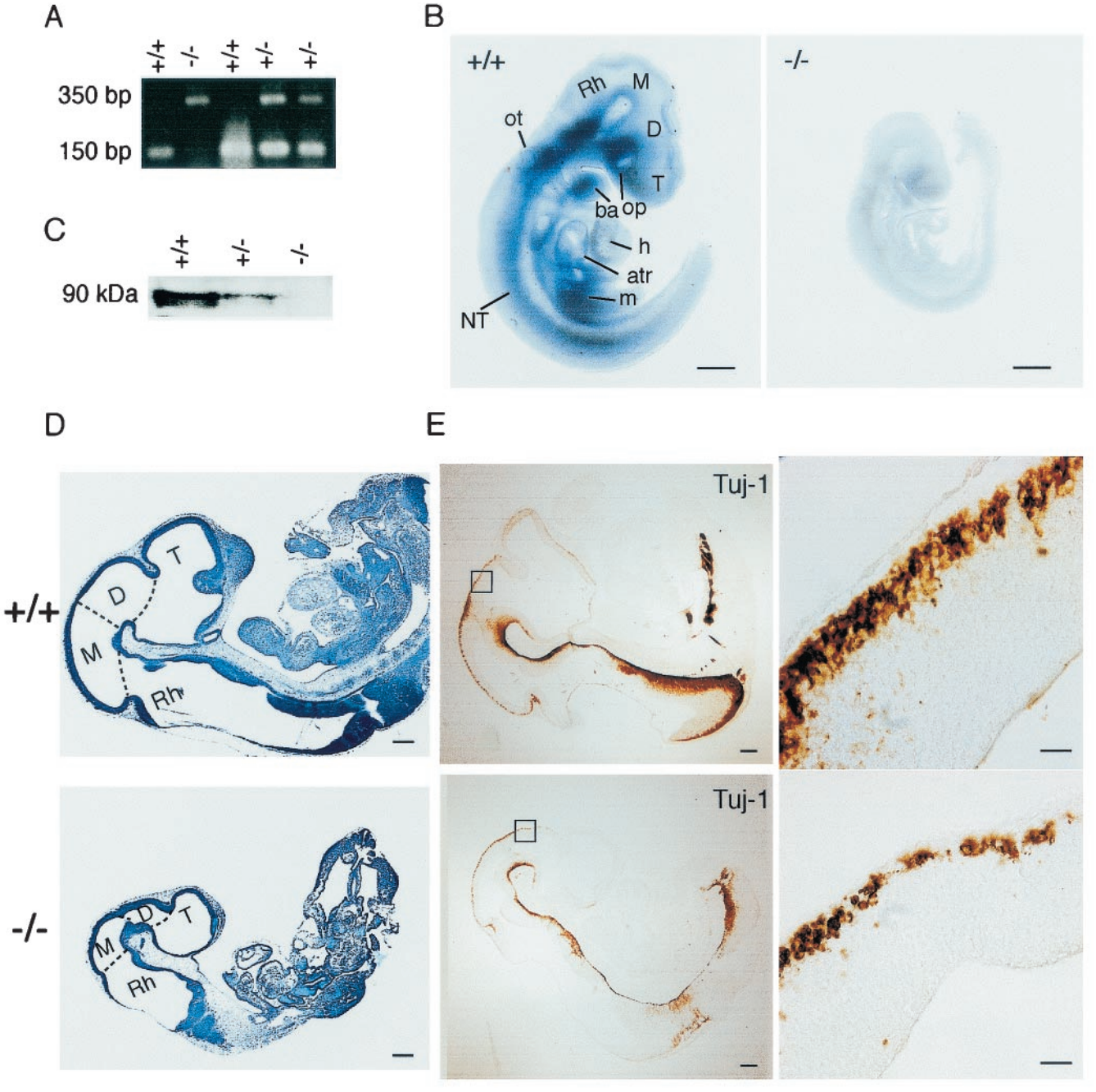

FIG. 2. Growth retardation of Dyrk1A$^{-/-}$ embryos. (A) Genotyping of wild-type (Dyrk1A$^{+/+}$), heterozygous (Dyrk1A$^{+/-}$), and homozygous (Dyrk1A$^{-/-}$) embryos by PCR analysis of DNA from embryonic yolk sac tissue. Locations of primers used for amplification of wild-type and targeted alleles are shown in Fig. 1B. (B) Whole-mount in situ hybridization in Dyrk1A$^{+/+}$ and Dyrk1A$^{-/-}$ E9.5 embryos using a riboprobe containing the deleted *Dyrk1A* sequence. The absence of signal in the Dyrk1A$^{-/-}$ embryo and its significant size reduction compared to the wild-type embryo can be appreciated. Bars, 1 mm. (C) Western blot analysis of equivalent amounts of protein extracts from Dyrk1A$^{+/+}$, Dyrk1A$^{+/-}$, and Dyrk1A$^{-/-}$ embryos with an anti-Dyrk1A specific antibody. The typical cluster of Dyrk1A bands around 90 kDa is shown. (D) Sagittal sections of cresyl violet-stained Dyrk1A$^{+/+}$ and Dyrk1A$^{-/-}$ embryos at E10.5. The differences between control and homozygous embryos in size and organ development, as well as in the proportions of the brain vesicles, can be appreciated. Bars, 1 mm. (E) (Left panels) Sagittal sections of E10.5 Dyrk1A$^{+/+}$ and Dyrk1A$^{-/-}$ embryos stained with an anti-β-tubulin antibody (Tuj-1) show a significant decrease in immunostaining for the mutant embryo. Bars, 2 mm. (Right panels) Areas within squares in left panels are amplified, showing fewer immunopositive postmitotic neurons in Dyrk1A$^{-/-}$ embryos than in wild-type embryos. Bars, 200 μm. Abbreviations: atr, common atrial chamber; ba, branchial arch; D, diencephalon; h, heart (truncus arteriosus and bulbus cordis); M, mesencephalon; m, mesodermal tissue; NT, neural tube; op, optic vesicle; ot, otic vesicle; Rh, rhombencephalon; T, telencephalon.

TABLE 1. Genotypes of embryos from Dyrk1A$^{+/-}$ matings

Day of gestation	No. of embryos	% Embryos			% Dead −/− embryos
		+/+	+/−	−/−	
9.5	39	13	61	26	0
10.5	93	29	50	21	20
11.5	143	27	53	20	45
12.5	36	31	44	25	67
13.5	12	33	25	42	80
14.5	6	17	83	0	100

difference between the two groups. In contrast, the body length curve of Dyrk1A$^{+/-}$ mice increased in parallel to that of their wild-type littermates. After weaning, both male and female Dyrk1A$^{+/-}$ mice presented a sustained lower body weight, with an average reduction of 30% (Fig. 3B and C).

To determine the effect of the mutation on organ size, we systematically weighed representative organs from adult heterozygous and control littermates. Although the brain and heart were lighter in Dyrk1A$^{+/-}$ mice, these decreases were proportional to the general decrease in body weight. On the other hand, the cerebellum (including the posterior mesencephalon) and liver presented disproportionate decreases in weight (Fig. 3C). This suggests that although Dyrk1A is ubiquitously expressed, the gene dose reduction influences the growth of different organs and tissues differentially. Gross histological examination of distinct organs revealed no obvious morphological abnormalities (data not shown).

Reduced brain size but normal cytoarchitectonics in most brain regions of Dyrk1A$^{+/-}$ mice. The brains of adult Dyrk1A$^{+/-}$ mice were about 30% smaller than those of respective wild-type mice and presented a remarkable macroscopic reduction in the mesencephalic tectum, which is composed of the superior and inferior colliculi (Fig. 4A). The rest of the brain regions were also decreased, although not in a homogeneous fashion. Nissl-stained sagittal sections revealed pronounced reductions in the midbrains and hindbrains of Dyrk1A$^{+/-}$ mice compared to forebrain structures such as the

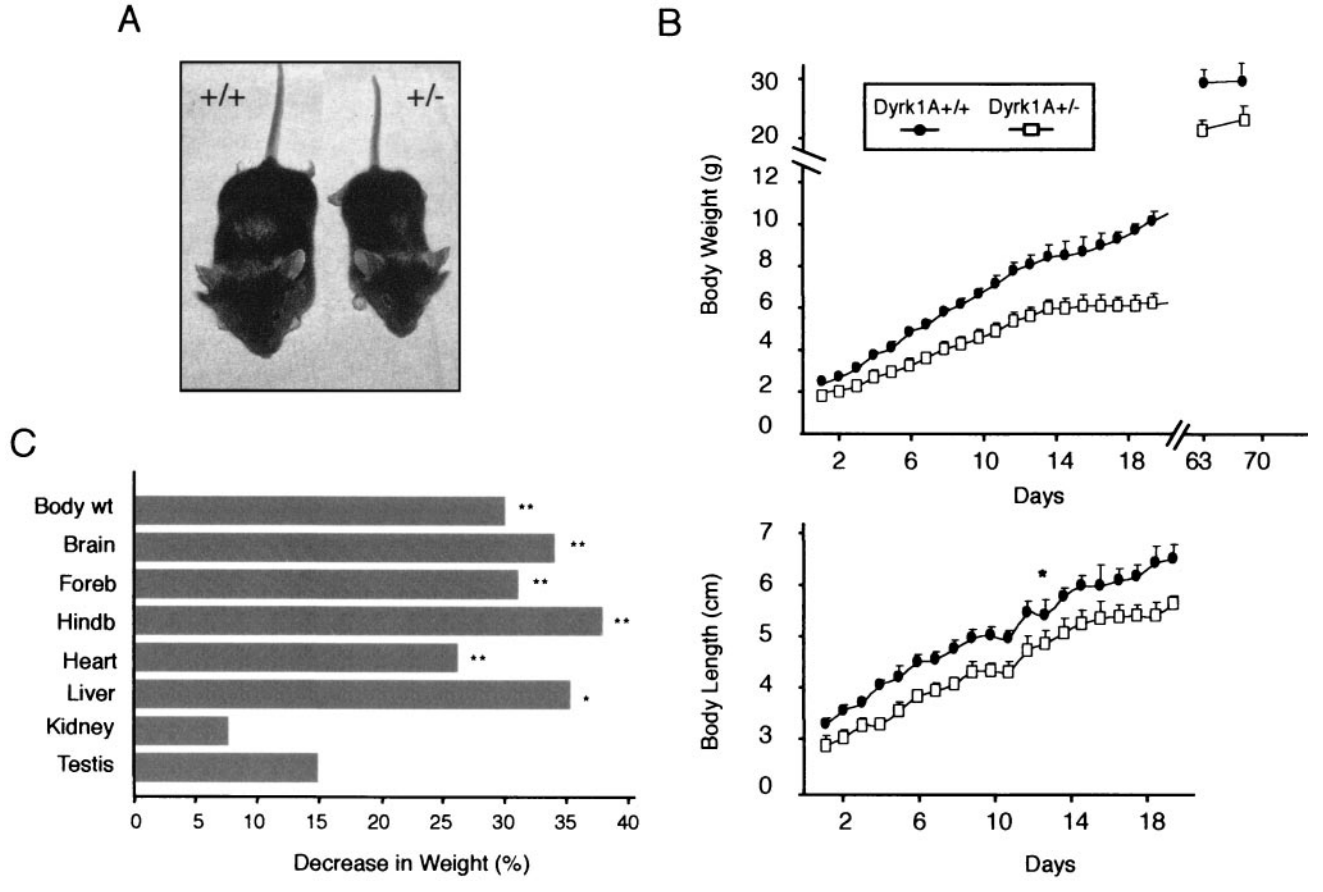

FIG. 3. Growth retardation and body size reduction of Dyrk1A$^{+/-}$ mice. (A) Comparison between a 1-month-old male wild-type mouse (+/+) and a heterozygous (+/−) littermate indicates the significant body reduction of the Dyrk1A$^{+/-}$ mouse. (B) Somatometric curves of preweaning mice. (Top) Weight gain retardation of Dyrk1A$^{+/-}$ mice early in life. Dyrk1A$^{+/-}$ mice remained underweight throughout life in comparison to their wild-type siblings. (Bottom) Growth retardation during early life in Dyrk1A$^{+/-}$ mice. Each data point represents a mean ± standard deviation. Data points for adult weights represent means of male weights. *, $P < 0.001$ by repeated-measures ANOVA; for all other data points, $P < 0.0001$ by repeated-measures ANOVA. (C) Percent decreases in body and organ weights in 3-month-old male Dyrk1A$^{+/-}$ mice relative to those of age-matched Dyrk1A$^{+/+}$ littermates. Asterisks indicate significant decreases in the body or net organ weight of Dyrk1A$^{+/-}$ mice ($n = 4$ mice per group; *, $P < 0.05$ by Student's t test; **, $P < 0.005$ by Student's t test). Abbreviations: wt, weight; Foreb, forebrain; Hindb, hindbrain and posterior part of mesencephalon.

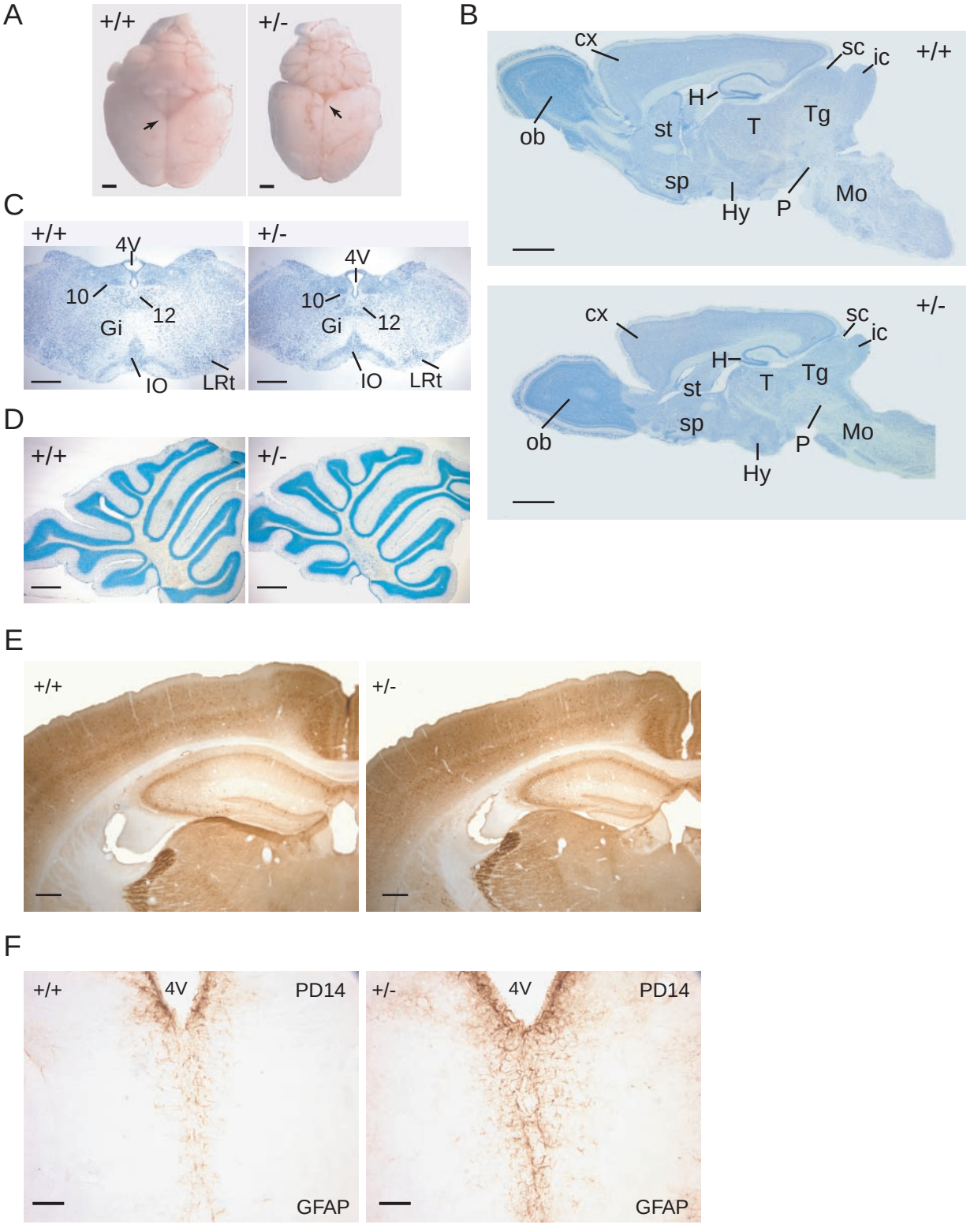

FIG. 4. Histological characterization of Dyrk1A$^{+/-}$ brains. (A) Dorsal views of brains of wild type (+/+) and Dyrk1A heterozygous (+/−) adult mice. Arrows point to the mesencephalic tectum, which is particularly decreased in +/− brains. Bars, 2 mm. (B) Nissl-stained sagittal sections of +/+ and +/− brains. Abbreviations: cx, cerebral cortex; H, hippocampus; Hy, hypothalamus; ic, inferior colliculus; Mo, medulla oblongata; ob, olfactory bulb; P, pons; sc, superior colliculus; sp, septum; st, striatum; T, thalamus; Tg, tegmentum. Bars, 2 mm. (C) Coronal sections of the medulla oblongata stained with Nissl. A significant decrease is observed in the Dyrk1A$^{+/-}$ section, although all nuclei (10, dorsal motor; 12, hypoglossal; Gi, gigantocellular reticular; IO, inferior olive; LRt, lateral reticular) are present. Bars, 500 μm. (D) Nissl-stained sagittal sections of +/+ and +/− cerebella. The layers and folia of the Dyrk1A$^{+/-}$ cerebellum are found normal. Bars, 500 μm. (E) Coronal sections of parvalbumin-immunostained brains reveal normal lamination of the Dyrk1A$^{+/-}$ cerebral cortex and hippocampus. Bars, 300 μm. (F) GFAP immunostaining in PD14 coronal brain sections shows increased GFAP immunoreactivity in Dyrk1A$^{+/-}$ mice. 4V, 4th ventricle. Bars, 75 μm.

TABLE 2. Neuronal counts from Dyrk1A$^{+/+}$ and Dyrk1A$^{+/-}$ brain regions

Region	Neuronal count[a] (mean ± SD)		P^b
	Dyrk1A$^{+/+}$	Dyrk1A$^{+/-}$	
Cortical layers II–III	200.5 ± 11.6	262.8 ± 34.5	< 0.0005
Cortical layer IV	243.7 ± 34.5	312.2 ± 66.4	0.015
Cortical layer V	114.8 ± 14.5	152.4 ± 11.6	< 0.0005
Thalamic VMP	133.3 ± 16.2	153.7 ± 8.3	0.03
SC			
SGS	268.5 ± 20.7	277.1 ± 24.3	0.46
SO	223.3 ± 45.9	252.3 ± 23.7	0.20

[a] Mean number of neurons per 10^6 μm^2 from four to eight different visual fields (50 μm thick) for each group.
[b] By Student's *t* test.

cerebral cortex and olfactory bulb (Fig. 4B). This is in accordance with the disproportionate reduction in weight of these brain regions (Fig. 3C). Furthermore, ventral brain regions, including the hypothalamus, pons, and medulla oblongata, were more severely affected than dorsal structures, such as the cerebellum or the neocortex (Fig. 4B, C, and D). These observations indicate a region-specific action of the mutation.

In spite of the differences in size, no obvious malformations were observed in the lamination of the olfactory bulb, neocortex, hippocampus, and cerebellar cortex (Fig. 4D) or in the structure of the striatum, thalamus, hypothalamus, and brain stem. Staining with antibodies against the major synaptic proteins SNAP 25, syntaxin 1, and synaptobrevin revealed that neither the expression of these proteins in the plexiform layers nor in the major axonal pathways were apparently altered in the brains of Dyrk1A$^{+/-}$ mice (data not shown). Immunostaining for the calcium-binding proteins calbindin D-28K, parvalbumin, and calretinin, which are used as markers for study of the CNS, showed that most neuronal subpopulations in Dyrk1A$^{+/-}$ mice exhibited normal distributions and immunoreactivities. For instance, Fig. 4E shows no difference between control and Dyrk1A$^{+/-}$ brains in the pattern of parvalbumin immunostaining in the cerebral cortex and hippocampus.

To evaluate a possible effect of Dyrk1A on the maturation of the CNS, similar immunohistochemical analyses were performed at PD14, an age at which a marked decrease in cortical calbindin D-28K-positive interneurons coincides with the emergence of parvalbumin immunoreactivity (1, 2). Again, the intensity and distribution of these neural markers were not altered in Dyrk1A$^{+/-}$ mice (data not shown). These findings reveal that although the brains of Dyrk1A$^{+/-}$ mice are reduced in size, most of the brain regions show normal cytoarchitectonics and neuronal components.

The macroglial cell populations of PD14 and adult brains were examined with antibodies against GFAP, an astroglial marker, and PLP, a marker of myelinated oligodendrocytes. Whereas GFAP staining was increased in all regions of both PD14 (Fig. 4F) and adult Dyrk1A$^{+/-}$ brains, no differences in

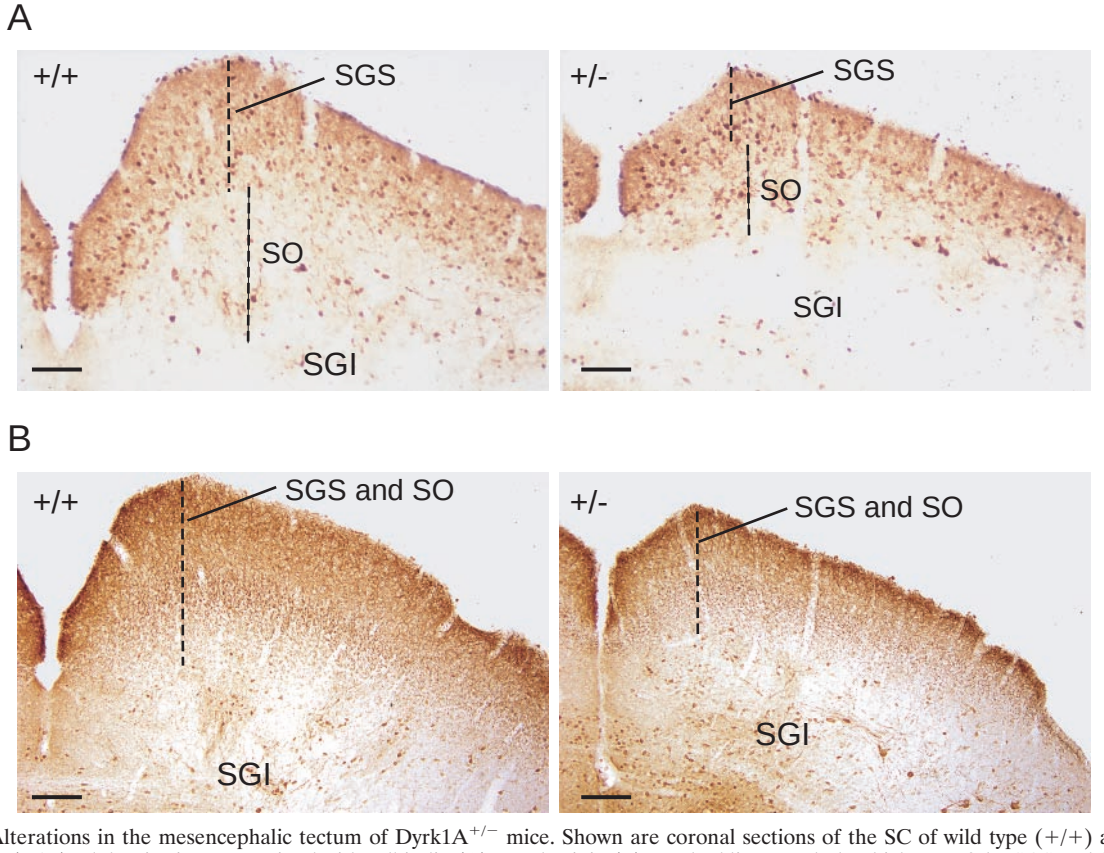

FIG. 5. Alterations in the mesencephalic tectum of Dyrk1A$^{+/-}$ mice. Shown are coronal sections of the SC of wild type (+/+) and Dyrk1A heterozygous (+/−) adult mice immunostained with calbindin (A) or calretinin (B). Dashed lines mark the thickness of the SGS and SO. The size reductions of these superficial layers in Dyrk1A$^{+/-}$ mice can be appreciated. SGI, stratum griseum intermedium. Bars, 100 μm.

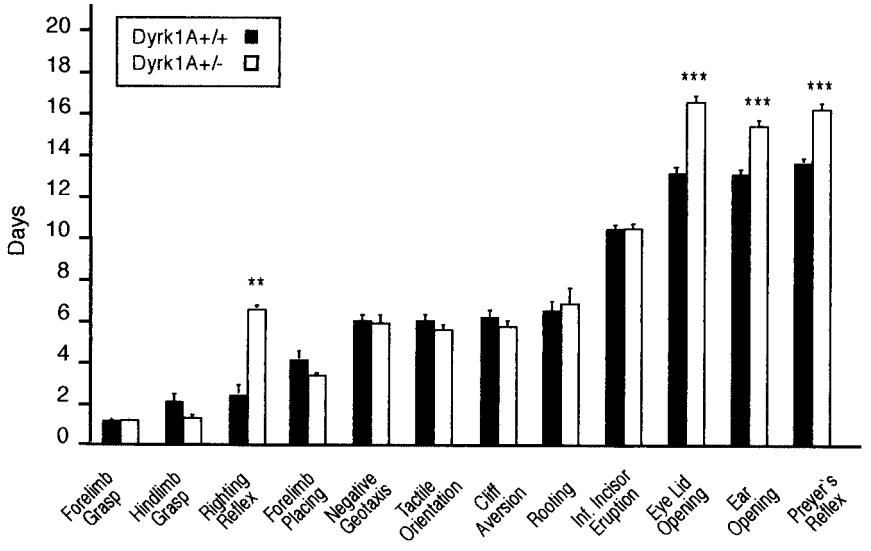

FIG. 6. Preweaning neurobehavioral analysis. Bars represent mean PDs for the emergence of physical landmarks or the achievement of mature responses in reflexological and behavioral tasks. **, $P < 0.001$ by Student's t test; ***, $P < 0.0001$ by Student's t test. Error bars, standard errors. Inf, inferior.

the pattern of PLP immunoreactivity between mutant and control brains were observed.

To evaluate possible alterations in cell body sizes that may account for the size reduction of Dyrk1A$^{+/-}$ brains, the areas of Nissl-stained neurons were measured in the neocortex, a brain region that presented moderate reduction, and the SC of the mesencephalic tectum, which presented severe reduction. No differences were observed between control and Dyrk1A$^{+/-}$ brains either in the pyramidal cells and the interneurons of layer V of the somatosensory barrel cortex (130.1 ± 54.8 μm^2 in Dyrk1A$^{+/-}$ mice versus 133.3 ± 53.5 μm^2 in controls; $P = 0.426$) or in neurons of the SGS of the SC (58.8 ± 23.5 μm^2 in Dyrk1A$^{+/-}$ mice versus 62.6 ± 24.2 μm^2 in controls; $P = 0.1$). Next, the densities of neuronal cells from different brain regions of control and Dyrk1A$^{+/-}$ mice were calculated. Neuronal densities in different layers of the somatosensory cortex and in the thalamic VPM nucleus were found to be significantly greater for Dyrk1A$^{+/-}$ mice than for controls (Table 2). This result indicates that the reduced size of these brain regions may be due to a decrease in the neuropil rather than to neuronal loss. In contrast, the neural densities of the SGS and the SO of the SC did not present significant differences between control and Dyrk1A$^{+/-}$ brains (Table 2). Immunostaining for the calcium-binding proteins revealed the presence of all major neuronal components of the SC. Nevertheless, staining with calbindin showed clearly that the sizes of SC superficial layers (SGS and SO) were severely reduced in Dyrk1A$^{+/-}$ brains (Fig. 5A). In addition, the density of calretinin-immunoreactive fibers, which are known to label retinofugal axons (14), was markedly decreased in the SGC and SO layers of Dyrk1A$^{+/-}$ brains (Fig. 5B). These results indicate that the reduced size of the SC is due to a reduction in the total number of neurons present in this region as well as to a decreased number of afferent fibers.

TABLE 3. SHIRPA primary behavioral assessment of adult Dyrk1A$^{+/-}$ mice

Test[a]	Score (mean)		Significance[b]
	Dyrk1A$^{+/+}$	Dyrk1A$^{+/-}$	
Body position	3.2	3.0	NS
Spontaneous activity	1.8	1.7	NS
Negative geotaxis	0.4	0.6	NS
Toe pinch	2.1	1.9	NS
Corneal reflex	1.5	2.1	NS
Visual placing	2.6	2.4	NS
Fear	1.0	1.0	NS
Irritability	0.8	0.6	NS
Freezing	1.3	1.8	$P = 0.05$
Startle response	3.0	2.4	$P = 0.03$

[a] Only tests relevant to the model are shown.
[b] By Student's t test. NS, not significant.

Neurobehavioral abnormalities of Dyrk1A$^{+/-}$ mice. The fact that DYRK1A may be involved in neurogenesis and may subsequently affect neurodevelopmental processes prompted us to analyze the neurobehavioral development of Dyrk1A$^{+/-}$ mice. Compared to their control littermates, these mice showed a significant delay in eyelid (PD 16.3 ± 0.28 versus PD 13.4 ± 0.16 in controls; $t = 9.39$ and $P < 0.0001$ by Student's t test) and ear (PD 15.6 ± 0.20 versus PD 13.6 ± 0.16; $t = 7.64$; $P < 0.0001$) opening. Examination of sensorial and motor reflexes revealed a significant delay in the appearance of the righting reflex in heterozygotes (PD 5.8 ± 1.01 versus PD 2.1 ± 0.35; $t = 4.03$; $P < 0.001$). This reflex evaluates the ability of the animal to turn from a supine to a prone position, and its acquisition depends on both muscular strength and neuromotor development. Chi-square analysis did not reveal any correlation between body weight and day of appearance of the righting reflex, thus excluding the reduced body weight of Dyrk1A$^{+/-}$ mice as a cause for the delay. A delay was also observed in the appearance of Preyer's reflex, an acoustically triggered reflex (PD 16.1 ± 0.26 versus PD 13.8 ± 0.13; $t = 8.72$; $P < 0.0001$), probably as a functional consequence of the

retarded ear opening of Dyrk1A$^{+/-}$ mice. Maturation of other neurological reflexes did not present any differences between the two groups (Fig. 6).

To assess neurobehavioral differences between Dyrk1A$^{+/+}$ and Dyrk1A$^{+/-}$ mice in adulthood, quantitative data about the performance of each individual were obtained from the primary screen of the SHIRPA protocol (28). Dyrk1A$^{+/-}$ mice were normal in most of the tests, but they presented prolonged freezing behavior compared to controls (score, 1.8 ± 0.13 versus 1.3 ± 0.24 in controls; t =-2.0; P = 0.05). The startle response was reduced in Dyrk1A$^{+/-}$ mice (score, 2.4 ± 0.23 versus 3.0 ± 0.01; t = 2.55; P = 0.03), while the visual placing test, which evaluates gross visual defects, was found normal. There was no significant effect of genotype on performance in tests measuring neuromuscular function, such as grip strength, limb tone, and wire maneuver, or in other sensory tests (tactile, proprioceptive, and nociceptive) (Table 3). These results suggest that the dose reduction of Dyrk1A causes specific neurological alterations.

DISCUSSION

Dyrk1A belongs to a novel subfamily of protein kinases (DYRKs) with unique structural and enzymatic features. In this study, we report the generation of a gene-targeting model for *Dyrk1A* and describe the phenotypic consequences of the loss of one and two copies of the gene.

Homozygous Dyrk1A$^{-/-}$ mice died during the period of organogenesis, between E10.5 and E13.5. Null embryos presented growth retardation, with reduction in body size and morphological developmental delay of the primitive organs, at the stages immediately prior to their deaths (E9.5 to E11.5). Many reported lethal mutants that die during this period present growth retardation defects, whereas for most, the cause of death is unknown. In general, the major developmental abnormalities that lead to death around the period of organogenesis include defective yolk sac circulation and failure to establish a chorioallantoic placenta, both leading to poor embryonic blood circulation (9). For the Dyrk1A$^{-/-}$embryos, the pale color of the yolk sac in most cases, as well as a swelling of the pericardium observed in some cases, suggests that defects in yolk sac hematopoiesis could be responsible for death.

The strong expression of *Dyrk1A* in the neural tube and the otic vesicle at E9.5, revealed by in situ hybridization analysis, suggests an important role for this gene during early stages of mouse nervous system development. The significant decrease in the number of postmitotic neural cells in Dyrk1A$^{-/-}$ embryos, revealed by β-tubulin immunostaining, is in accordance with the general developmental delay of the null embryos. However, the possibility that the loss of *Dyrk1A* could lead to a nervous system defect, related either to a reduction in the number of neuroblasts or to a deregulation of neural differentiation, should also be considered.

Newborn heterozygotes showed reduced neonatal viability and a decrease in the body size of surviving mice, while heterozygous embryos at E9.5 to E11.5 presented normal gross morphology. This suggests that although the reduction in Dyrk1A protein amounts is not sufficient to limit viability and growth during the period of organogenesis, Dyrk1A is critical for normal growth of the pups. The observation of growth delay as early as PD1 indicates that it arises from an intrinsic intrauterine retardation during the last stages of gestation, when rodent *Dyrk1A* is highly expressed (27). The increased difference in weight between Dyrk1A$^{+/-}$ pups and their wild-type counterparts during the last week of the preweaning period suggests that the growth delay might be dependent not only on intrinsic genetic factors but also on a poorer adaptive response. This growth defect affects both sexes similarly and is not overcome in adulthood. Interestingly, a similar size reduction has been described for adult *mnb* flies (34).

During the preweaning period, when essential processes of brain regionalization and acquisition of functional competence are taking place, fundamental sensory-motor abilities are acquired. Among the different reflexes that determine motor coordination and balance (righting reflex, negative geotaxis, and cliff aversion), a significant delay was observed only in the appearance of the righting reflex in Dyrk1A$^{+/-}$ pups. All of these reflexes depend mainly on the cerebellovestibular system and arise at different time points during the preweaning period (23). The appearance of the righting reflex coincides with enhanced expression of rodent Dyrk1A in the cerebellum observed when important developmental processes are taking place (27), and this could account for the specific delay of this reflex produced by Dyrk1A dose reduction. Again, the developmental delay of Dyrk1A$^{+/-}$ mice presents an analogy to the longer time that *mnb* flies need for development (34).

During adulthood, Dyrk1A$^{+/-}$ mice exhibit normal spontaneous behavior in general, as revealed by the SHIRPA primary analysis. The enhanced freezing response suggests increased anxiety or, alternatively, changes in the emotional behavior of Dyrk1A$^{+/-}$ mice. On the other hand, the poorer reactivity of Dyrk1A$^{+/-}$ mice, shown by the lower score on Preyer's reflex, indicates an acoustic deficit, which might be related to the retarded appearance of this reflex during the preweaning period. Thus, the Dyrk1A dose reduction does not result in gross neurological defects but rather in subtle alterations that may involve specific CNS functional domains.

Human *DYRK1A* has been proposed as a candidate gene for some of the neurological defects observed in DS patients. This notion has been supported by its mapping position in the DS critical region, its ubiquitous expression in the adult and embryonic nervous systems (16, 27, 29, 32), its overexpression in the brains of DS patients (15), and the neurobehavioral alterations shown by transgenic mice overexpressing the gene (3, 30). Taken together, these data indicate the involvement of *DYRK1A* in CNS function. Nevertheless, the only morphological evidence about its essential role in the CNS so far comes from *Drosophila* mutants with reduced mnb expression, resulting in flies with small brain size (34). A remarkable effect of mouse *Dyrk1A* haploinsufficiency was a disproportionate brain reduction, providing strong evidence about the functional importance of the gene in the development of the mammalian CNS. The prominent decreases in the posteroventral brains of adult Dyrk1A$^{+/-}$ mice coincide with high-level expression of *Dyrk1A* during early embryonic development in the posteroventral neural tube (rhombencephalon and spinal cord). The normal histological patterns of the brain structures of Dyrk1A$^{+/-}$ mice, together with a disproportionate reduction in specific areas, are analogous to the lack of significant architectural abnormalities and to the presence of region-specific

brain reductions in *mnb* flies, respectively (34). Interestingly, a functional analogy exists between two structures that are found disproportionately reduced in the mouse and fly mutants. The SC presents a horizontal laminated organization and is a major target of retinal ganglion cells, while the optic lobe is a three-layered structure that receives the input of the photoreceptor cells of the *Drosophila* ommatidia (10). Therefore, the high degree of phenotypic resemblance between Dyrk1A$^{+/-}$ and *mnb* mutants suggests a conserved role of the DYRK1A kinase in the function of the nervous system.

The significant increases in the cell densities of the somatosensory cortex and thalamus of the Dyrk1A$^{+/-}$ brain suggest a tighter arrangement of neuronal cells. This could result either from reductions in neurite complexity and in the size of the soma or from a decrease in the surrounding glia. No differences in the area of the soma were revealed between the two groups, while there was an increase in the number of GFAP-positive cells in Dyrk1A$^{+/-}$ brains, indicating an increase in the astroglial population. The recent finding that overexpression of a kinase-deficient DYRK1A attenuates the neurite outgrowth of hippocampal cells after bFGF stimulation (37) indicates that Dyrk1A dose reduction could affect the length and complexity of the neuropil. Thus, we propose that the decreases in the sizes of the somatosensory cortex and thalamus of the Dyrk1A$^{+/-}$ brain are outcomes of the crowding of neuronal cells, probably due to a decrease in the arborization of the neuropil.

In contrast to the above observations, the densities of the neuronal populations in the SGS and the SO of the SC were found unchanged, indicating that the remarkable reductions in the sizes of these layers in Dyrk1A$^{+/-}$ brains may result from a reduction in neuronal cell numbers. In addition, immunostaining with calretinin revealed a significant reduction in the number of retinal cell afferents of the SGS and SO layers, suggesting decreased fiber number as an additional cause for the reductions in the sizes of these layers. We and others (32) have observed high *Dyrk1A* expression in the optic vesicle during embryonic development, suggesting that the dose reduction of the *Dyrk1A* gene could cause a specific defect in the developing retina. In contrast, *Dyrk1A* is moderately expressed in the dorsal mesencephalic vesicle, from which the mesencephalic tectum will derive. Considering these data, we suggest that reductions in Dyrk1A protein levels lead to reductions in the numbers of retinofugal fibers in the SGS and the SO layers of Dyrk1A$^{+/-}$ brains and to subsequent decreases in the numbers of neurons in these layers.

Minimal deletions in the region where human *DYRK1A* maps have been described in partial monosomy 21 (MO-21) patients (24), who present microcephaly, mental retardation, intrauterine and postnatal growth retardation, and characteristic physical features (8). Dyrk1A$^{+/-}$ mice present reductions in brain size, possible intrauterine growth retardation, and postnatal growth retardation, resulting from targeted deletion of one allele. The striking phenotypic similarities between Dyrk1A$^{+/-}$ mice and MO-21 patients suggest that some of the characteristic features of MO-21 could be directly related to the dose reduction of *DYRK1A* and that Dyrk1A$^{+/-}$ mice should be considered as a possible mouse model for the study of microcephaly.

In conclusion, the mortality of Dyrk1A$^{-/-}$ embryos and the alterations in Dyrk1A$^{+/-}$ mice support the vital, nonredundant role of Dyrk1A. The phenotype of Dyrk1A$^{+/-}$ provides evidence about the role of Dyrk1A in cellular mechanisms that determine body growth and development. In the CNS, Dyrk1A is involved in the determination of the size of the brain, probably through mechanisms that control neural differentiation. The notable resemblance of the effects of its loss in the Dyrk1A$^{+/-}$ mouse to those in the *mnb* mutant fly suggests a conserved function, emphasizing its biological importance along the phylogenetic tree.

ACKNOWLEDGMENTS

We thank S. de la Luna, C. Fillat, and E. Varea for helpful comments on the manuscript, M. Pritchard and J. Guimerà for valuable advice during the initial design of the project, the staff of the animal facility, M. Ródenas for technical contributions to the histology of the mouse embryos, M. Martínez de Lagrán for help with the SHIRPA analysis, and B. Zalc for the antibody against PLP.

This work was supported by grants from the Spanish Ministry of Education and Science (SAF99-0092-01), the European Union (CEC/BIOMED2 BMH4-CT98-3039), and the Lejeune Foundation. V.F. was supported by a TMR Marie Curie Research Training Grant (contract ERBFMBICT972278).

REFERENCES

1. **Alcantara, S., L. de Lecea, J. A. Del Rio, I. Ferrer, and E. Soriano.** 1996. Transient colocalization of parvalbumin and calbindin D28k in the postnatal cerebral cortex: evidence for a phenotypic shift in developing nonpyramidal neurons. Eur. J. Neurosci. **8:**1329–1339.
2. **Alcantara, S., I. Ferrer, and E. Soriano.** 1993. Postnatal development of parvalbumin and calbindin D28K immunoreactivities in the cerebral cortex of the rat. Anat. Embryol. (Berlin) **188:**63–73.
3. **Altafaj, X., M. Dierssen, C. Baamonde, E. Marti, J. Visa, J. Guimera, M. Oset, J. R. Gonzalez, J. Florez, C. Fillat, and X. Estivill.** 2001. Neurodevelopmental delay, motor abnormalities and cognitive deficits in transgenic mice overexpressing Dyrk1A (minibrain), a murine model of Down's syndrome. Hum. Mol. Genet. **10:**1915–1923.
4. **Bahler, J., and J. R. Pringle.** 1998. Pom1p, a fission yeast protein kinase that provides positional information for both polarized growth and cytokinesis. Genes Dev. **12:**1356–1370.
5. **Becker, W., and H. G. Joost.** 1999. Structural and functional characteristics of Dyrk, a novel subfamily of protein kinases with dual specificity. Prog. Nucleic Acid Res. Mol. Biol. **62:**1–17.
6. **Becker, W., Y. Weber, K. Wetzel, K. Eirmbter, F. J. Tejedor, and H. G. Joost.** 1998. Sequence characteristics, subcellular localization, and substrate specificity of DYRK-related kinases, a novel family of dual specificity protein kinases. J. Biol. Chem. **273:**25893–25902.
7. **Campbell, L. E., and C. G. Proud.** 2002. Differing substrate specificities of members of the DYRK family of arginine-directed protein kinases. FEBS Lett. **510:**31–36.
8. **Chettouh, Z., M. F. Croquette, B. Delobel, S. Gilgenkrants, C. Leonard, C. Maunoury, M. Prieur, M. O. Rethore, P. M. Sinet, M. Chery, et al.** 1995. Molecular mapping of 21 features associated with partial monosomy 21: involvement of the APP-SOD1 region. Am. J. Hum. Genet. **57:**62–71.
9. **Copp, A. J.** 1995. Death before birth: clues from gene knockouts and mutations. Trends Genet. **11:**87–93.
10. **Cutforth, T., and U. Gaul.** 1997. The genetics of visual system development in *Drosophila*: specification, connectivity and asymmetry. Curr. Opin. Neurobiol. **7:**48–54.
11. **Davisson, M. T., C. Schmidt, and E. C. Akeson.** 1990. Segmental trisomy of murine chromosome 16: a new model system for studying Down syndrome. Prog. Clin. Biol. Res. **360:**263–280.
12. **Fox, W. M.** 1965. Reflex-ontogeny and behavioural development of the mouse. Anim. Behav. **13:**234–241.
13. **Garrett, S., M. M. Menold, and J. R. Broach.** 1991. The *Saccharomyces cerevisiae* YAK1 gene encodes a protein kinase that is induced by arrest early in the cell cycle. Mol. Cell. Biol. **11:**4045–4052.
14. **Gobersztejn, F., and L. R. Britto.** 1996. Calretinin in the mouse superior colliculus originates from retinal ganglion cells. Braz. J. Med. Biol. Res. **29:**1507–1511.
15. **Guimera, J., C. Casas, X. Estivill, and M. Pritchard.** 1999. Human minibrain homologue (MNBH/DYRK1): characterization, alternative splicing, differential tissue expression, and overexpression in Down syndrome. Genomics **57:**407–418.
16. **Guimera, J., C. Casas, C. Pucharcos, A. Solans, A. Domenech, A. M. Planas,**

J. Ashley, M. Lovett, X. Estivill, and M. A. Pritchard. 1996. A human homologue of *Drosophila* minibrain (MNB) is expressed in the neuronal regions affected in Down syndrome and maps to the critical region. Hum. Mol. Genet. **5:**1305–1310.
17. **Hanks, S. K., and A. M. Quinn.** 1991. Protein kinase catalytic domain sequence database: identification of conserved features of primary structure and classification of family members. Methods Enzymol. **200:**38–62.
18. **Henrique, D., J. Adam, A. Myat, A. Chitnis, J. Lewis, and D. Ish-Horowicz.** 1995. Expression of a Delta homologue in prospective neurons in the chick. Nature **375:**787–790.
19. **Himpel, S., P. Panzer, K. Eirmbter, H. Czajkowska, M. Sayed, L. C. Packman, T. Blundell, H. Kentrup, J. Grotzinger, H. G. Joost, and W. Becker.** 2001. Identification of the autophosphorylation sites and characterization of their effects in the protein kinase DYRK1A. Biochem. J. **359:**497–505.
20. **Kentrup, H., W. Becker, J. Heukelbach, A. Wilmes, A. Schurmann, C. Huppertz, H. Kainulainen, and H. G. Joost.** 1996. Dyrk, a dual specificity protein kinase with unique structural features whose activity is dependent on tyrosine residues between subdomains VII and VIII. J. Biol. Chem. **271:**3488–3495.
21. **Kuhn, R., K. Rajewsky, and W. Muller.** 1991. Generation and analysis of interleukin-4-deficient mice. Science **254:**707–710.
22. **Laemmli, U. K.** 1970. Cleavage of structural proteins during the assembly of the head of bacteriophage T4. Nature **227:**680–685.
23. **Le Roy, I., F. Perez-Diaz, A. Cherfouh, and P. L. Roubertoux.** 1999. Preweaning sensorial and motor development in laboratory mice: quantitative trait loci mapping. Dev. Psychobiol. **34:**139–158.
24. **Matsumoto, N., H. Ohashi, M. Tsukahara, K. C. Kim, E. Soeda, and N. Niikawa.** 1997. Possible narrowed assignment of the loci of monosomy 21-associated microcephaly and intrauterine growth retardation to a 1.2-Mb segment at 21q22.2. Am. J. Hum. Genet. **60:**997–999.
25. **Matsuo, R., W. Ochiai, K. Nakashima, and T. Taga.** 2001. A new expression cloning strategy for isolation of substrate-specific kinases by using phosphorylation site-specific antibody. J. Immunol. Methods **247:**141–151.
26. **Miyata, Y., and E. Nishida.** 1999. Distantly related cousins of MAP kinase: biochemical properties and possible physiological functions. Biochem. Biophys. Res. Commun. **266:**291–295.
27. **Okui, M., T. Ide, K. Morita, E. Funakoshi, F. Ito, K. Ogita, Y. Yoneda, J. Kudoh, and N. Shimizu.** 1999. High-level expression of the Mnb/Dyrk1A gene in brain and heart during rat early development. Genomics **62:**165–171.
28. **Rogers, D. C., E. M. Fisher, S. D. Brown, J. Peters, A. J. Hunter, and J. E. Martin.** 1997. Behavioral and functional analysis of mouse phenotype: SHIRPA, a proposed protocol for comprehensive phenotype assessment. Mamm. Genome **8:**711–713.
29. **Shindoh, N., J. Kudoh, H. Maeda, A. Yamaki, S. Minoshima, Y. Shimizu, and N. Shimizu.** 1996. Cloning of a human homolog of the *Drosophila minibrain*/rat *Dyrk* gene from "the Down syndrome critical region" of chromosome 21. Biochem. Biophys. Res. Commun. **225:**92–99.
30. **Smith, D. J., M. E. Stevens, S. P. Sudanagunta, R. T. Bronson, M. Makhinson, A. M. Watabe, T. J. O'Dell, J. Fung, H. U. Weier, J. F. Cheng, and E. M. Rubin.** 1997. Functional screening of 2 Mb of human chromosome 21q22.2 in transgenic mice implicates minibrain in learning defects associated with Down syndrome. Nat. Genet. **16:**28–36.
31. **Song, W. J., S. H. Chung, and D. M. Kurnit.** 1997. The murine Dyrk protein maps to chromosome 16, localizes to the nucleus, and can form multimers. Biochem. Biophys. Res. Commun. **231:**640–644.
32. **Song, W. J., L. R. Sternberg, C. Kasten-Sportes, M. L. Keuren, S. H. Chung, A. C. Slack, D. E. Miller, T. W. Glover, P. W. Chiang, L. Lou, and D. M. Kurnit.** 1996. Isolation of human and murine homologues of the *Drosophila* minibrain gene: human homologue maps to 21q22.2 in the Down syndrome "critical region." Genomics **38:**331–339.
33. **Souza, G. M., S. Lu, and A. Kuspa.** 1998. YakA, a protein kinase required for the transition from growth to development in *Dictyostelium*. Development **125:**2291–2302.
34. **Tejedor, F., X. R. Zhu, E. Kaltenbach, A. Ackermann, A. Baumann, I. Canal, M. Heisenberg, K. F. Fischbach, and O. Pongs.** 1995. *minibrain*: a new protein kinase family involved in postembryonic neurogenesis in *Drosophila*. Neuron **14:**287–301.
35. **Woods, Y. L., P. Cohen, W. Becker, R. Jakes, M. Goedert, X. Wang, and C. G. Proud.** 2001. The kinase DYRK phosphorylates protein-synthesis initiation factor eIF2Bε at Ser539 and the microtubule-associated protein tau at Thr212: potential role for DYRK as a glycogen synthase kinase 3-priming kinase. Biochem. J. **355:**609–615.
36. **Woods, Y. L., G. Rena, N. Morrice, A. Barthel, W. Becker, S. Guo, T. G. Unterman, and P. Cohen.** 2001. The kinase DYRK1A phosphorylates the transcription factor FKHR at Ser329 in vitro, a novel in vivo phosphorylation site. Biochem. J. **355:**597–607.
37. **Yang, E. J., Y. S. Ahn, and K. C. Chung.** 2001. Protein kinase Dyrk1 activates cAMP response element-binding protein during neuronal differentiation in hippocampal progenitor cells. J. Biol. Chem. **276:**39819–39824.